ACS APPLIED MATERIALS & INTERFACES

RESEARCH ARTICLE

www.acsami.org

Facile Control of C_2H_5OH Sensing Characteristics by Decorating Discrete Ag Nanoclusters on SnO_2 Nanowire Networks

In-Sung Hwang,[†] Joong-Ki Choi,[†] Hyung-Sik Woo,[†] Sun-Jung Kim,[†] Se-Yeon Jung,[†] Tae-Yeon Seong,[†] Il-Doo Kim,[‡] and Jong-Heun Lee*[,†]

[†]Department of Materials Science and Engineering, Korea University, Seoul 136-713, Republic of Korea

[‡]Department of Materials Science and Engineering, Korea Advanced Institute of Science and Technology, Daejeon 305-701, Republic of Korea

Supporting Information

ABSTRACT: The effect of Ag decoration on the gas sensing characteristics of SnO_2 nanowire (NW) networks was investigated. The Ag layers with thicknesses of 5−50 nm were uniformly coated on the surface of SnO_2 NWs via e-beam evaporation, which were converted into isolated or continuous configurations of Ag islands by heat treatment at 450 °C for 2 h. The SnO_2 NWs decorated by isolated Ag nano-islands displayed a 3.7-fold enhancement in gas response to 100 ppm C_2H_5OH at 450 °C compared to pristine SnO_2 NWs. In contrast, as the Ag decoration layers became continuous, the response to C_2H_5OH decreased significantly. The enhancement and deterioration of the C_2H_5OH sensing characteristics by the introduction of the Ag decoration layer were strongly governed by the morphological configurations of the Ag catalysts on SnO_2 NWs and their sensitization mechanism.

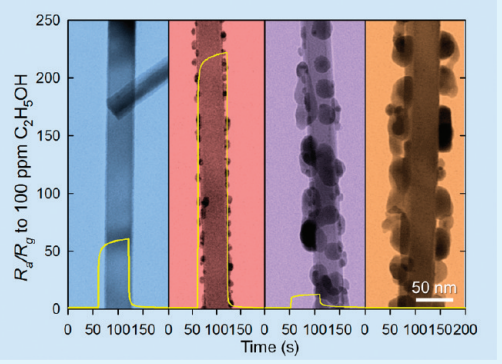

KEYWORDS: SnO_2, nanowires, gas sensor, Ag catalyst, electronic sensitization

1. INTRODUCTION

Oxide nanowires (NWs) with large surface-to-volume ratios and high crystallinity show promising gas sensing characteristics, such as a high gas response and excellent thermal stability.[1−6] Compared to the individual NW counterparts, NW networks exhibit higher gas responses because of the significant chemoresistive variation at the contacts between NWs.[7−10] NWs tend to form a less agglomerated configuration of networked structures, whereas nanoparticles are easily aggregated into large secondary particles due to strong van der Waals attractions. Thus, analyte gases can diffuse rapidly and effectively toward the entire sensing surface via porous NW network structures, which enhance both the gas response and gas responding speed simultaneously.[11]

The gas sensitivity, selectivity, and response/recovery speed can be enhanced, tuned, and designed by the addition of noble metal or metal oxide additives.[12,13] Porous and less agglomerated NW networks are also advantageous for the uniform loading of sensitizers. To date, noble metal catalysts, such as Pd,[14−20] Pt,[21,22] and Au,[23−25] and oxide additives, such as CuO,[26,27] Co_3O_4,[28] and La_2O_3,[29] have been loaded onto SnO_2, ZnO, In_2O_3, and WO_3 NWs to improve their gas sensing characteristics. Although the effect of Ag loading on gas sensing characteristics of TiO_2 nanobelts has been reported recently,[30] to the best of our knowledge, the role of the relatively economic Ag catalyst in the gas sensing behaviors of SnO_2 NWs has barely been investigated.

It has been reported that gas sensing characteristics of NWs are significantly influenced by the loading method, loading amount, morphology, and sensitization mechanism of catalysts.[31,32] Thus, in this contribution, Ag catalysts with different sizes, amounts, and connecting configurations were loaded onto SnO_2 NWs by e-beam evaporation of Ag metal and subsequent heat treatment to investigate the effect of Ag loading on the gas response, gas responding/recovering kinetics, and resistance in air of a SnO_2 NW network sensor. The main focus of this paper is directed at the elucidation of the gas sensing mechanism of Ag-loaded SnO_2 NWs in conjunction with the facile control of the space charge modulation depth by the configuration variations of Ag nano-islands.

2. EXPERIMENTAL SECTION

The SnO_2 NWs were synthesized by thermal evaporation using Sn metal powder. The Au(30 Å)-coated Si substrate was placed downstream of the source material in a quartz tube. The pressure of the processing tube was maintained at $\sim 1 \times 10^{-2}$ Torr by mechanical pumping. SnO_2 NWs were grown at 700 °C for 20 min with an O_2 flow rate of 0.5 sccm (Figure 1a). The Ag layers with different thicknesses (5, 10, and 50 nm) were coated onto the SnO_2 NWs by e-beam evaporation (Figure 1b,c). The thickness of Ag layer was measured during evaporation using thin film deposition thickness monitor (STM-100/MF, Sycon Instruments, Inc., USA).

Received: May 20, 2011
Accepted: July 11, 2011
Published: July 11, 2011

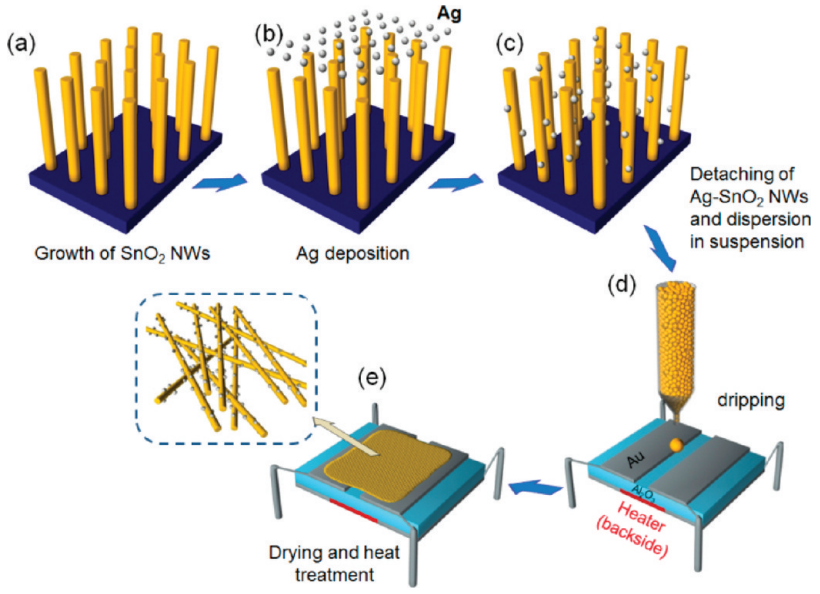

Figure 1. Schematic diagram illustrating fabrication procedure of Ag-decorated SnO_2 NW network gas sensors.

The pure and Ag-coated SnO_2 NWs were detached from the Si substrate, dispersed in isopropanol (Sigma−Aldrich Co., Ltd., USA) by ultrasonic treatment, dried at 80 °C for 24 h, and mixed with organic binders (ethyl cellulose: α-terpinol = 1:14 by wt%). The suspension containing Ag-coated SnO_2 NWs was dropped using a micropipet onto Al_2O_3 substrates (size: 1.5 × 1.5 mm^2, thickness: 0.25 mm) with two Au electrodes on their top surfaces (electrode width: 1 mm, spacing between electrodes: 0.2 mm) and a micro-heater on each of their bottom surfaces (Figure 1d). The sensor was heated at 450 °C for 2 h in air to remove any residual organic content (Figure 1e). Hereinafter, for simplicity, the Ag-decorated SnO_2 NW network sensors prepared by coating of Ag layers with thicknesses of 5 nm, 10 nm, and 50 nm and subsequent heat treatment (450 °C for 2 h in air) will be referred as "5Ag-SnO_2", "10Ag-SnO_2", and "50Ag-SnO_2" sensors, respectively.

The sensor element was packaged with a stainless steel holder and the sensor temperature was controlled by modulating the power of the microheater underneath the substrate. The sensor was contained within a specially designed quartz tube with a very small volume (1.5 cm^3) to minimize the time of atmospheric change. A detailed experimental setup for measuring gas response is shown elsewhere.[33] The gas responses (R_a/R_g; R_a, resistance in air; R_g, resistance in analyte gas) to 100 ppm C_2H_5OH, NH_3, H_2, and CO were measured at 450 °C. The gas concentration was controlled by changing the mixing ratio of the parent gases (200 ppm C_2H_5OH, 200 ppm NH_3, 200 ppm H_2, and 200 ppm CO, all in air balance) and dry synthetic air. The dc 2-probe resistance of the sensor was measured using an electrometer that was interfaced with a computer.

The morphology and structure of the pure SnO_2 and Ag-decorated SnO_2 NWs were characterized with X-ray diffraction (XRD, Rigaku D/MAX-2500 V/PC), field emission scanning electron microscopy (FESEM, Hitachi S-4300), transmission electron microscopy, energy-dispersive X-ray spectroscopy, and selected area electron diffraction (TEM/EDX/SAED, JEOL JEM-3011). The chemical state of Ag-decorated SnO_2 NWs was analyzed by X-ray photoelectron spectroscopy (XPS, ULVAC-PHI, PHI 5000, Versa Probe).

3. RESULTS AND DISCUSSION

As-grown SnO_2 NWs were 50−100 nm thick and several tens of micrometers long with clear surfaces (Figure 2a). After a 5 nm thick Ag layer deposition and subsequent heat treatment

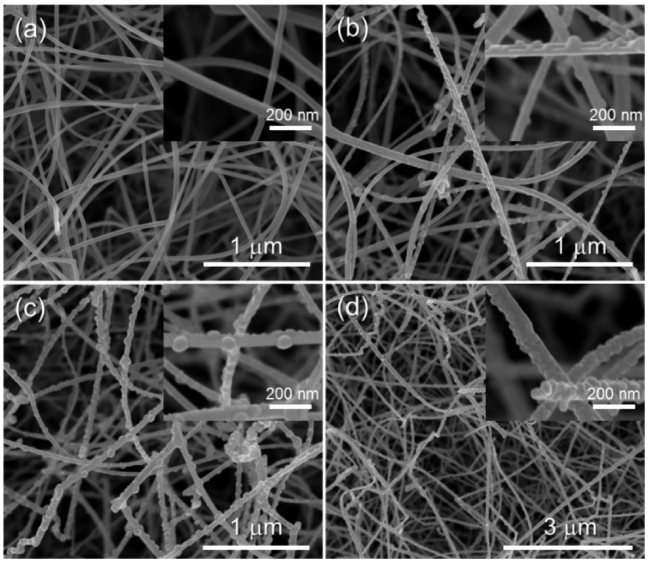

Figure 2. Scanning electron micrographs of (a) pure SnO_2 NW networks, (b) 5Ag-SnO_2 NW networks, (c) 10Ag-SnO_2 NW networks, and (d) 50Ag-SnO_2 NW networks after heat treatment at 450 °C for 2 h.

at 450 °C in air, the surfaces of the NWs became rough (Figure 2b). The Ag nanoparticles became larger and covered more surfaces of the NWs in the 10Ag-SnO_2 (Figure 2c) and 50Ag-SnO_2 specimens (Figure 2d).

The pure SnO_2 rutile phase was found in the X-ray diffraction pattern (see Figure S1 in the Supporting Information). No significant Ag or Ag-based oxide such as AgO and Ag_2O peak was found in the 5Ag-SnO_2 and 10Ag-SnO_2 NWs, probably because of the low detection limit of X-ray diffraction. In 50Ag-SnO_2 NWs, the Ag (200) peak was observed. No Ag_2O peak was detected in all specimens.

The size and configuration of the Ag nanoparticles on the SnO_2 NWs were investigated in detail using TEM (Figure 3). Considering the clean surface morphology of the pure SnO_2 NWs (Figure 3a), the spotty configuration of the nano-islands

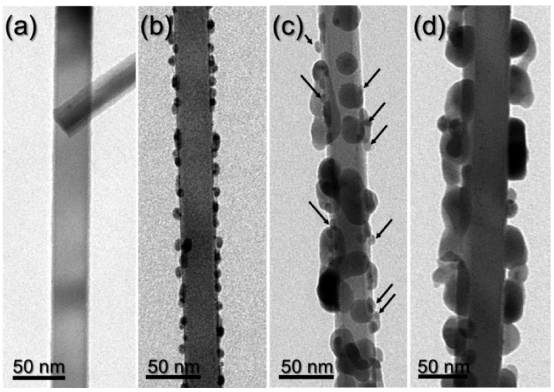

Figure 3. Transmission electron micrographs of (a) pure SnO_2 NW networks, (b) 5Ag-SnO_2 NW networks, (c) 10Ag-SnO_2 NW networks, and (d) 50Ag-SnO_2 NW networks after heat treatment at 450 °C for 2 h.

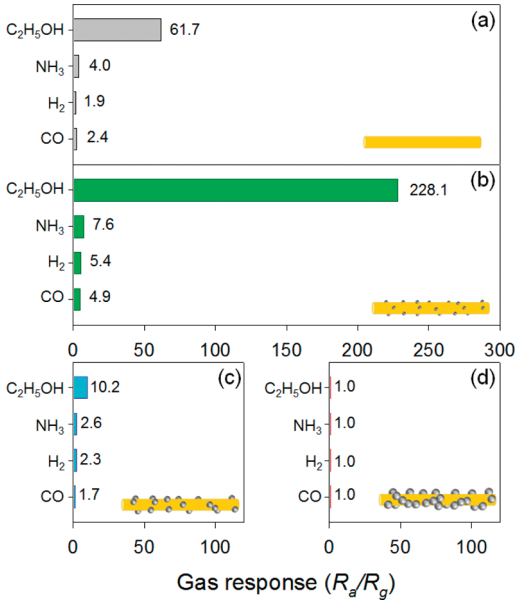

Figure 4. Gas responses to 100 ppm C_2H_5OH, NH_3, H_2, and CO at 450 °C of: (a) pure SnO_2 NW sensor; (b) 5Ag-SnO_2 NW sensor; (c) 10Ag-SnO_2 NW sensor; (d) 50Ag-SnO_2 NW sensor.

found in Ag-doped SnO_2 NW specimens is attributed to Ag-based nanoparticles, which was confirmed by EDS analysis (see Figure S2 in the Supporting Information). The diameters of the Ag nanoparticles ranged from 8 to 15 nm in the 5Ag-SnO_2 specimen (Figure 3b), which increased to 20−40 nm in the 10Ag-SnO_2 specimen (Figure 3c), although nanoparticles (arrows in Figure 3c) with smaller diameters were also observed. In the 50Ag-SnO_2 specimen, the Ag nanoparticles on the SnO_2 NWs became coarsened to the size range of 30 - 60 nm (Figure 3d). Note that the Ag nanoparticles in the 50Ag-SnO_2 specimen are connected in a continuous manner, whereas those in the 5Ag-SnO_2 specimen are decorated in rather discrete forms.

The presence and chemical states of Sn, O, and Ag elements in 5Ag-SnO_2 and 50Ag-SnO_2 specimens were confirmed by XPS analysis (see Figure S3 in the Supporting Information). The concentrations of Ag in 5Ag-SnO_2 and 50Ag-SnO_2 specimens were determined to be 0.92 and 3.35 at%, respectively. Hoflund et al. (34) reported that the binding energies of Ag in Ag, Ag_2O, and AgO are 368.3, 367.9, and 367.3 eV, respectively. Thus the Ag $3d_{5/2}$ peak at 367.9 eV can be attributed to Ag in Ag_2O. Considering the Ag peak in the XRD pattern of 50Ag-SnO_2 specimen (see Figure S1 in the Supporting Information), both Ag and Ag_2O phases coexisted on outer surface of SnO_2 NWs. However, it was still difficult to confirm the co-existence of AgO from XPS spectra due to the close location of three Ag $3d_{5/2}$ peaks in Ag, Ag_2O, and AgO.

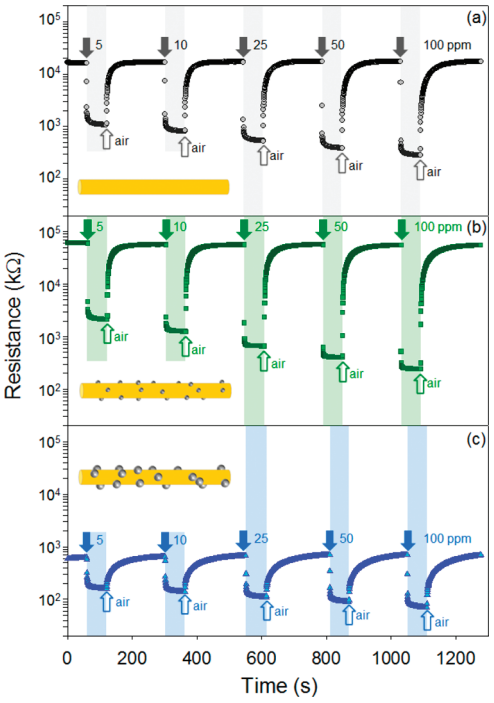

Figure 5. Dynamic C_2H_5OH sensing transients of (a) pure SnO_2 NW sensor, (b) 5Ag-SnO_2 NW sensor, and (c) 10Ag-SnO_2 NW sensor at 450 °C.

The response ($S = R_a/R_g$) of the pure SnO_2 NW network sensor to 100 ppm C_2H_5OH at 450 °C was 61.7, which was significantly higher than the responses to 100 ppm NH_3, H_2, and CO (1.9−4.0) (Figure 4a). In the 5Ag-SnO_2 sensor, the R_a/R_g value to 100 ppm C_2H_5OH dramatically increased to 228.1, whereas those to other gases increased slightly (4.9−7.6) (Figure 4b). The selectivity to C_2H_5OH was defined as the response ratio between gas response to 100 ppm C_2H_5OH and that to other interference gas ($S_{ethanol}/S_{gas}$). The $S_{ethanol}/S_{gas}$ values for NH_3, H_2, and CO were 15.4−31.5 in pure SnO_2 NW network sensor (see Figure S4 in the Supporting Information). These values increased to 30.0−46.6 in 5Ag-SnO_2 sensor. This result clearly indicates that the decoration of Ag nanoparticles is very effective for enhancing not only gas response but also selectivity to C_2H_5OH. However, further coating of Ag nanoparticles decreased the response to C_2H_5OH down to 10.2 in the case of 10Ag-SnO_2 sensor (Figure 4c). The responses to other gases were also reduced significantly and the $S_{ethanol}/S_{gas}$ values for NH_3, H_2, and CO became low (3.9−6.0) compared to those of pure SnO_2 and 10Ag-SnO_2 sensors (see Figure S4 in the Supporting Information). Finally, the gas responses to all gases vanished completely in the 50Ag-SnO_2 sensor due to the continuous nature of Ag layer (Figure 4d).

The sensing transients of pure SnO_2, 5Ag-SnO_2, and 10Ag-SnO_2 NW sensors to 5−100 ppm C_2H_5OH are given in Figure 5.

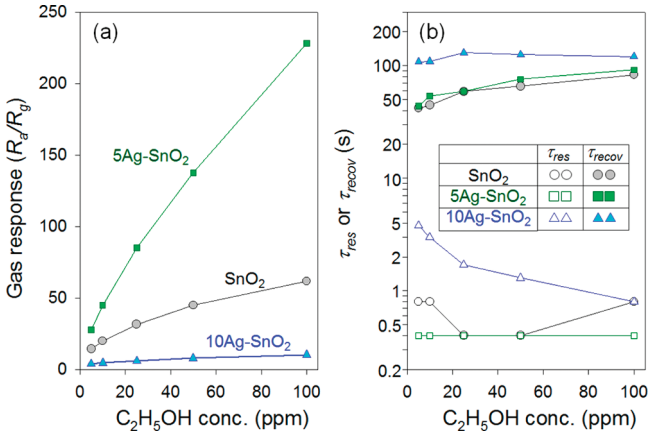

Figure 6. (a) C_2H_5OH responses (R_a/R_g) and (b) 90% response and recovery times (τ_{res} and τ_{recov}) of SnO_2, 5Ag-SnO_2, and 10Ag-SnO_2 NW sensors.

All the sensors exhibited the typical n-type gas sensing behaviors upon exposure to C_2H_5OH. Their sensor resistances decreased when exposed to C_2H_5OH and returned to the original value when exposed to air in a reproducible manner. The times to reach 90% variation in resistance upon exposure to C_2H_5OH and air were defined as the 90% response time (τ_{res}) and the 90% recovery time (τ_{recov}), respectively. The R_a/R_g, τ_{res}, and τ_{recov} values were calculated from the sensing transients (Figure 5) and the results are summarized in Figure 6. The responses of the pure SnO_2 NW sensor to 5−100 ppm C_2H_5OH ranged from 14.2 to 61.7, which increased to 27.8−228.1 in the 5Ag-SnO_2 NW sensor (Figure 6a). To the contrary, the responses to 5−100 ppm C_2H_5OH decreased to 3.9−10.2 in the 10Ag-SnO_2 NW sensor (Figure 6a).

In the literature, Ag catalysts are known to enhance the responses of oxide semiconductors either by an electronic and/or chemical sensitization mechanism.[31,35−45] The former enhances the gas response by extension of the electron depletion layer beneath the Ag decoration layer.[31,35−37] The latter is known to promote the gas response reaction by the dissociation of reducing gases via a spillover mechanism.[40,41] Therefore, the configuration of the Ag layer and its consequent effect on the R_a values are very important for understanding the gas responses in Figures 4−6. The R_a value of the pure SnO_2 NW sensor was 16.5 MΩ (Figure 5a). The R_a value increased to 61.8 MΩ by the coating of 5 nm thick Ag layer and subsequent heat treatment (Figure 5b). The variation in the sensor resistance for 5 different pure SnO_2 NW network sensors was smaller than 30%. Thus, the ∼3.7 times increase in R_a in the 5Ag-SnO_2 specimen indicates the presence of an electronic interaction between the Ag and SnO_2 NWs. In general, the electronic sensitization of sensors involves a redox reaction between Ag_2O and Ag[12,31,35] and the consequent change of its energy band diagram at the interface between Ag_2O/Ag and oxide semiconductors. A small amount of Ag_2O layer, which was confirmed by XPS analysis, can exist at the surface of the Ag nanoparticles, which is enough to extend the electron depletion layer in an air atmosphere.

The remarkable increase in R_a by the introduction of discrete Ag islands on the surface of SnO_2 NWs strongly supports this idea. The chemical sensitization via the spillover mechanism cannot be excluded as a reason for the enhancement of gas response, although further studies are necessary.

The R_a value decreased significantly to 590 kΩ in the 10Ag-SnO_2 NW sensor (Figure 5c). From the TEM image in Figure 3c, the significant decrease of R_a can be attributed to the partial connection between the Ag coating layer and/or Ag particles. Finally, the R_a value decreased dramatically down to 1.9 Ω in the 50Ag-SnO_2 NW sensor, which is explained by the complete connection between the metallic Ag particles and/or Ag layers. When the Ag islands are partially or completely connected with each other, the sensor resistance is not governed by gas sensing properties of SnO_2 NWs, but instead it is determined by the insensitive conducting Ag layer. Thus, negligible or no gas responses in the 10Ag-SnO_2 and 50Ag-SnO_2 NW sensors are attributed to the formation of conducting channels by the Ag layers. These results are consistent with the literature data that show the enhancement and deterioration of the gas response induced by low and high loading concentrations of Ag catalysts, respectively.[37,38,44,45] This clearly shows that both the loading concentration and the connecting configuration of the Ag catalysts are very important in promoting gas sensing characteristics.

The τ_{res} values of the pure SnO_2 and 5Ag-SnO_2 NW sensors were very short (0.4 − 0.8 s) (Figure 6a), while those of the 10Ag-SnO_2 NW sensor were relatively high (1−5 s) (Figure 6b). The τ_{recov} values of the pure SnO_2 and 5Ag-SnO_2 NW sensors were also very similar (40−80 s) in the entire C_2H_5OH concentration range, whereas those of the 10Ag-SnO_2 NW sensor were higher (∼100 s). The rapid response characteristics indicate that the in-diffusion of reducing gas toward the sensor surface occurs very rapidly through the less-agglomerated network structures and the subsequent oxidation reaction of the reducing gas by the negatively charged surface oxygen is also very quick. Taking into account the rapid diffusion of gas, the sluggish recovery should be understood as the slow surface reactions relating to the adsorption, dissociation, and ionization of oxygen molecules on the surface of the sensor. The most plausible reason for the longer τ_{res} and τ_{recov} values of the 10Ag-SnO_2 NW sensor is the prevention of the gas sensing reaction on SnO_2 NWs due to the coating of a wider area with Ag catalysts. Accordingly, as shown with the 5Ag-SnO_2 NW sensor with a discrete configuration of Ag nano-islands, the gas response may be significantly enhanced without the deterioration of gas responding/recovering speed.

From the above results, the gas sensing mechanism of the pure SnO_2 and 5Ag-SnO_2 NW network sensors can be given as follows: In the pure SnO_2 NW network, the electron depletion layer forms on the surface of the crystalline oxide NWs by the adsorption of negatively charged oxygen, which leads to the formation of a resistive-semiconducting core-shell structure (Figure 7a, left). Thus, the conduction in an individual oxide NW is described by parallel competition between the semiconducting core and resistive shell layers. The reducing gas is oxidized by the reaction with negatively charged surface oxygen, which leads to the increase of conductivity (Figure 7a, right). However, under this parallel conduction model, it is difficult to achieve a very high gas response when the diameters of NWs are significantly large because the conduction through semiconducting core (insensitive part) dominates over the chemoresistive variation along the near-surface shell layer.

In contrast, the decoration of Ag islands in a discrete manner can extend the electron depletion to the deeper layer of NWs by the electronic sensitization mechanism (Figure 7b, left). Thus, a bigger cross section of the NWs is changed into the electron depletion layer and the resistance of the NW is governed by the regions with the narrowest semiconducting cross-section. Upon

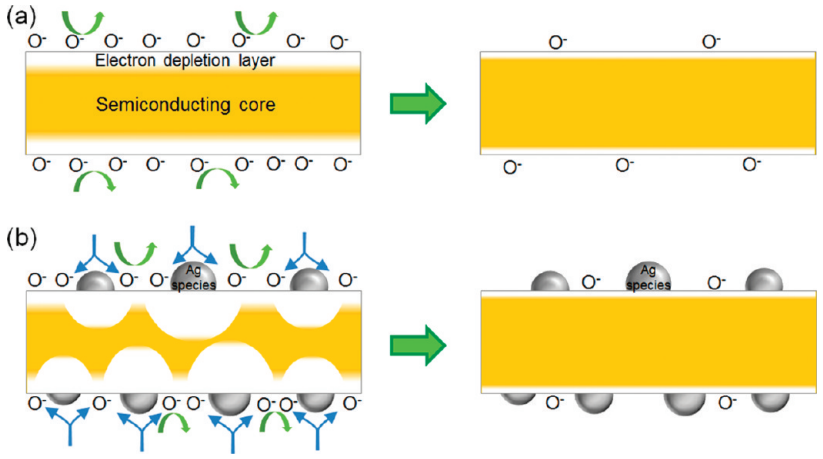

Figure 7. Schematic diagrams on the gas sensing mechanism of (a) pure SnO_2 NWs and (b) Ag-decorated SnO_2 NWs.

exposure to reducing gases, the deep electron depletion layer underneath the Ag nanoparticles changes into a shallow layer, which leads to a significant enhancement in gas response (Figure 7b, right). In the real applications of Ag-decorated SnO_2 NW network sensors, the migration of Ag clusters at the sensing temperature should be taken into account as a possible reason to affect the long-term stability.[46] Finally, the heavy loading of the Ag catalyst with a continuous configuration leads to the deterioration of the gas response by conduction along the metallic Ag particles regardless of chemoresistive variation.

5. CONCLUSIONS

The effect of Ag loading on the gas sensing characteristics of SnO_2 NW network sensors was investigated. The decoration of NW networks with the discrete configuration of Ag nanoparticles significantly enhanced the response and selectivity to C_2H_5OH without the deterioration of gas responding/recovering speeds. This was explained by the increase in resistance in air via the electronic interaction between Ag and SnO_2 NWs. When the Ag nanoparticles became partially or completely connected with each other, the gas response significantly decreased or vanished, which was attributed to conduction through the highly conductive Ag particles regardless of chemoresistive variation. This clearly shows that the size, concentration, and connecting configuration of decorative Ag nanoparticles are very important for enhancing the gas sensing characteristics of SnO_2 NWs.

■ ASSOCIATED CONTENT

Supporting Information. X-ray diffraction patterns, energy dispersive X-ray spectroscopy results, X-ray photoelectron spectroscopy results, and selective gas sensing characteristics of pristine and Ag-decorated SnO_2 nanowires. This material is available free of charge via the internet at http://pubs.acs.org/.

■ AUTHOR INFORMATION

Corresponding Author

*E-mail: jongheun@korea.ac.kr. Fax: +82-2-928-3584. Tel: +82-2-3290-3282.

■ ACKNOWLEDGMENT

This work was supported by KOSEF NRL program grant funded by the Korean government (MEST) (R0A-2008-000-20032-0) and the Fundamental R&D program for Core Technology of Materials (M2008010013) funded by Ministry of Knowledge Economy.

■ REFERENCES

(1) Comini, E. *Anal. Chim. Acta* **2006**, *568*, 28–40.
(2) Kolmakov, A.; Moskovits, M. *Annu. Rev. Mater. Res.* **2004**, *34*, 151–180.
(3) Wan, Q.; Li, Q. H.; Chen, Y. J.; Wang, T. H.; He, X. L.; Li, J. P.; Lin, C. L. *Appl. Phys. Lett.* **2004**, *84*, 3654–3656.
(4) Comini, E.; Faglia, G.; Sberveglieri, G.; Pan, Z. W.; Wang, Z. L. *Appl. Phys. Lett.* **2002**, *81*, 1869–1871.
(5) Kolmakov, A.; Zhang, Y.; Cheng, G.; Moskovits, M. *Adv. Mater.* **2003**, *15*, 997–1000.
(6) Sysoev, V. V.; Schneider, T.; Goschnick, J.; Kiselev, I.; Habicht, W.; Hahn, H.; Strelcov, E.; Kolmakov, A. *Sens. Actuators, B* **2009**, *138*, 699–703.
(7) Zhang, D.; Liu, Z.; Li, C.; Tang, T.; Liu, X.; Han, S.; Lei, B.; Zhou, C. *Nano Lett.* **2004**, *4*, 1919–1924.
(8) Hwang, I.-S.; Kim, Y.-S.; Kim, S.-J.; Ju, B.-K.; Lee, J.-H. *Sens. Actuators, B* **2009**, *136*, 224–229.
(9) Choi, Y.-J .; Hwang, I.-S.; Park, J.-G.; Choi, K. J.; Park, J.-H.; Lee, J.-H. *Nanotechnology* **2008**, *19*, 095508.
(10) Kahn, R.; Ra, H.-W.; Kim, J. T.; Jang, W. S.; Sharma, D.; Im, Y. H. *Sens. Actuators B* **2010**, *150*, 389–393.
(11) Hwang, I.-S.; Lee, E.-B.; Kim, S.-J.; Choi, J.-K.; Cha, J.-H.; Lee, H.-J.; Ju, B.-K.; Lee, J.-H. *Sens. Actuators, B* **2011**, *154*, 295−300.
(12) Yamazoe, N.; Kurosawa, Y.; Seiyama, T. *Sens. Actuators* **1983**, *4*, 283–289.
(13) Kim, H.-R.; Choi, K.-I.; Kim, K.-M.; Kim, I.-D.; Cao, G.; Lee, J.-H. *Chem. Commun.* **2010**, *46*, 5061–5063.
(14) Kolmakov, A.; Klenov, D.O.; Lilach, Y.; Stemmer, S.; Moskovits, M. *Nano Lett.* **2005**, *5*, 667–673.
(15) Yang, D.-J.; Kamienchick, I.; Youn, D. Y.; Rothchild, A.; Kim, I. −D. *Adv. Funct. Mater.* **2010**, *20*, 4258–4264.
(16) Shen, Y.; Yamazaki, T.; Liu, Z.; Meng, D.; Kikuta, T.; Nakatani, N.; Saito, M.; Mori, M. *Sens. Actuators, B* **2009**, *135*, 524–529.
(17) Lee, J. M.; Park, J.-E.; Kim, S.; Kim, S.; Lee, E.; Kim, S.-J.; Lee, W. *Int. J. Hydrogen Energy* **2010**, *35*, 12568–12573.
(18) Zhang, Y.; Xiang, Q.; Xu, J.; Xu, P.; Pan, Q.; Li, F. *J. Mater. Chem.* **2009**, *19*, 4701–4706.
(19) Hsueh, T.-S.; Chang, S.-J.; Hsu, C. L.; Lin, Y.-R.; Chen, I.-C. *Appl. Phys. Lett.* **2007**, *91*, 053111.
(20) Kim, S. S.; Park, J. Y.; Choi, S.-W.; Kim, H. S.; Na, H. G.; Yang, J. C.; Kim, H. W. *Nanotechnology* **2010**, *21*, 415502.

(21) Zhang, Y.; Xu, J.; Xu, P.; Zhu, Y.; Chen, X.; Yu, W. *Nanotechnology* **2010**, *21*, 285501.
(22) Zhan, L. F.; She, J. C.; Luo, J. Y.; Deng, S. Z.; Chen, J.; Xu, N. S. *J. Phys. Chem. C* **2010**, *114*, 15504–15509.
(23) Joshi, R. K.; Hu, Q.; Alvi, F.; Joshi, B.; Kumar, A. *J. Phys. Chem. C* **2009**, *113*, 16199–16202.
(24) Chang, S.-J.; Hsueh, T.-J.; Chen, I.-C.; Hsieh, S. F.; Chang, S.-P.; Hsu, C.-L.; Lin, Y.-R.; Huang, B.-R. *IEEE Trans. Nanotechnol.* **2008**, *7*, 754–759.
(25) Vallejos, S.; Stoycheva, T.; Umek, P.; Navio, C.; Snyders, R.; Bittencourt, C.; Llobet, E.; Blackman, C.; Moniz, S.; Correig, X. *Chem. Commun.* **2011**, *47*, 565–567.
(26) Hwang, I.-S.; Choi, J.-K.; Kim, S.-J.; Dong, K.-Y.; Kwon, J.-H.; Zu, B.-K.; Lee, J.-H. *Sens. Actuators B* **2009**, *142*, 105–110.
(27) Kumar, W.; Sen, S.; Muthe, K. P.; Gaur, N. K.; Gupta, S. K.; Yakhimi, J. V. *Sens. Actuators B* **2009**, *138*, 587–590.
(28) Na, C.-W.; Woo, H.-S.; Kim, I.-D.; Lee, J.-H. *Chem. Commun.* **2011**, *47*, 5148–5150.
(29) Hieu, N. V.; Kim, H.-R.; Lee, J.-H. *Sens. Actuators, B* **2008**, *133*, 228–234.
(30) Hu, P.; Du, G.; Zhou, W.; Cui, J.; Lin, J.; Liu, H.; Liu, D.; Wang, J.; Chen, S. *ACS Appl. Mater. Interfaces* **2010**, *2*, 3263–3269.
(31) Yamazoe, N. *Sens. Actuators, B* **1991**, *S*, 7–19.
(32) Koziej, D.; Barsan, N.; Shimanoe, K.; Yamazoe, N.; Scuber, J.; Weimar, U. *Sens. Actuators B* **2006**, *118*, 98–104.
(33) Choi, J.-K.; Hwang, I.-S.; Kim, S.-J.; Park, J.-S.; Park, S.-S.; Jeong, U.; Kang, Y. C.; Lee, J.-H. *Sens. Actuators, B* **2010**, *150*, 191–199.
(34) Hoflund, G. B.; Hazoe, Z. F.; Salaita, G. N. *Phys. Rev. B.* **2000**, *62*, 11126–11132.
(35) Singh, V. N.; Mehta, B. R.; Joshi, R. K.; Kruis, F. E.; Shivaprasad, S. M. *Sens. Actuators B* **2007**, *125*, 482–488.
(36) Matsushima, S.; Teraoka, Y.; Miura, N.; Yamazoe, N. *Jpn. J. Appl. Phys.* **1988**, *27*, 1798–1802.
(37) Zhang, J.; Colbow, K. *Sens. Actuators, B* **1997**, *40*, 47–52.
(38) Xiang, Q.; Meng, G.; Zhang, Y.; Xu, J.; Xu, P.; Pan, Q.; Yu, W. *Sens. Actuators B* **2000**, *143*, 635–640.
(39) Joshi, R. K.; Krius, F. E. *Appl. Phys. Lett.* **2006**, *89*, 153116.
(40) Joshi, R. K.; Krius, F. E.; Dmitrieva, O. *J. Nanoparticle Res.* **2006**, *8*, 797–808.
(41) Sun, Z.-P.; Liu, L.; Zhang, L.; Jia, D.-Z. *Nanotechnology* **2006**, *17*, 2266–2270.
(42) Hu, P.; Du, G.; Zhou, W.; Cui, J.; Lin, J.; Liu, H.; Liu, D.; Wang, J.; Chen, S. *ACS Appl. Mater. Interfaces* **2010**, *2*, 3263–3269.
(43) Wen, Z.; Tian-mo, L.; De-jun, L. *Physica B* **2010**, *405*, 4235–4239.
(44) Wang, J.; Zou, B.; Ruan, S.; Zhao, J.; Wu, F. *Mater. Chem. Phys.* **2009**, *117*, 489–493.
(45) Wang, Y.; Wang, Y.; Cao, J.; Kong, F.; Xia, H.; Zhang, J.; Zhu, B.; Wang, S.; Wu, S. *Sens. Actuators, B* **2008**, *131*, 183–189.
(46) Sears, W. M.; Love, D. A. *Phys. Rev. B* **1993**, *47*, 12792–12795.